

Combining mechanical and thermal surface fourier transform analysis to follow the dynamic fatigue behavior of polymers

Valerian Hirschberg^{a,b}, Manfred Wilhelm^b, Denis Rodrigue^{a,*}

^a Department of Chemical Engineering and CERMA, Université Laval, 1065 Avenue de La Médecine, Quebec, G1V 0A6, Canada

^b Institute for Chemical Technology and Polymer Chemistry, Karlsruhe Institute of Technology (KIT), Engesserstraße 18, 76131, Karlsruhe, Germany

ARTICLE INFO

Keywords:

Mechanical fatigue
Nonlinear stress response
Plasticity
Thermoelastic coupling
Intrinsic heating

ABSTRACT

This work investigates the phenomena of self-heating, also called intrinsic heating, and thermoelastic coupling during non-linear dynamic mechanical fatigue testing via surface temperature measurement coupled with the mechanical behavior of polymers. Static tensile tests and dynamic strain controlled fatigue tests under tension/tension were performed at a frequency of $\omega_1/2\pi = 5$ Hz, as well as in the low cycle fatigue regime at $\omega_1/2\pi = 0.2$ Hz, on six polymers: high density polyethylene (HDPE), low density polyethylene (LDPE), ultra high molecular weight polyethylene (UHMWPE), polyamide 6 (PA6), and two grades of polypropylene (PP).

In dynamic testing, the surface temperature rises to a plateau value (ΔT) when an equilibrium between the viscous/plastic dissipated energy and heat convection is reached. Power-law correlations were found between the strain amplitude (ϵ_0) and ΔT , as well as between ϵ_0 and the calculated dissipated energy density ($W_{diss,p}$) obtained from the mechanical stress response, with similar exponents for both correlations. Thermoelastic coupling is firstly investigated in uniaxial tension, revealing a linear relation between the strain rate and the rate of temperature decrease, which is more distinct with decreasing polymer chain mobility. In dynamic fatigue testing, the surface temperature was found to oscillate with an amplitude T_1 , which was analyzed via Fourier transform. A direct relation between T_1 and ϵ_0 at small deformations was observed. At large strain amplitudes, T_1 (ϵ_0) follows a similar trend as the complex modulus $E^*(\epsilon_0)$. At low frequencies and large strain amplitudes, additional higher harmonics at two (T_2) and three (T_3) times the fundamental frequency were also detected as fingerprints of plastic deformation, resulting in additional heat dissipated during the loading half cycle. From the results obtained, the advantages of the calculated dissipated energy density over the surface temperature analysis was analyzed to predict the fatigue behavior. This analysis is believed to be valid for all materials due to the mathematical/physical principles involved. The results are thus expected to hold for other materials such as composites, rubbers, ceramics and metals.

1. Introduction

Viscoelastic materials dissipate energy under cyclic deformation as the viscous part of the stress response is dissipated into heat, while the elastic part of the applied work is stored. During cyclic loading (fatigue), this results in an increase of the surface temperature of the sample due to cyclic loading (intrinsic heating) and a constant value (plateau) is reached at equilibrium between heat dissipation and convection loss to the environment. Intrinsic heating is of high importance in fatigue testing as the stress (σ) response of a material is related to its temperature:

$$\sigma = \sigma(T) \quad (1)$$

This is even more important for polymers above or close to their glass transition temperature (T_g) as they soften with increasing temperature. For strain-controlled oscillatory deformation in tension/tension, the time dependent strain can be written in a simplified complex notation as:

$$\epsilon(t) = \epsilon_s + \epsilon_d = \epsilon_s + \epsilon_0 e^{i\omega_1 t} \quad (2)$$

with the static (ϵ_s) and the sinusoidal oscillatory dynamic (ϵ_d) part of the deformation. A direct proportionality can be observed in the linear regime (small deformation) between the deformation of a sample and its stress response ($\sigma \propto \epsilon$). In this case the stress can be written as:

* Corresponding author.

E-mail address: denis.rodrigue@gch.ulaval.ca (D. Rodrigue).

$$\sigma = I_0 + I_1 e^{i\omega_1 t + \delta_1} \quad (3)$$

where I_0 is the average stress intensity (different than zero under tension), I_1 is the stress amplitude and δ_1 its phase angle [1]. In the linear regime, the material properties of a viscoelastic material can be completely defined by the storage (E') and loss (E'') moduli as:

$$E' = \frac{I_1}{\varepsilon_0} \cos(\delta_1) \quad (4)$$

$$E'' = \frac{I_1}{\varepsilon_0} \sin(\delta_1) \quad (5)$$

The storage modulus is proportional to the elastically stored energy, while the loss modulus is proportional to the energy lost, which can (mechanically) not be regained (irreversible). The energy lost is mainly dissipated as heat, so the dissipated energy density (normalized by the sample volume) during each cycle, is proportional to the loss modulus E'' or the area enclosed by a hysteresis loop, the so-called Lissajous curve [1]. This energy loss can be described as (see Appendix A):

$$W_{diss} = \int_{\varepsilon^-}^{\varepsilon^+} \sigma d\varepsilon = \pi \varepsilon_0^2 E'' \quad (6)$$

For the linear regime, when E'' is independent of the applied strain amplitude, Eq. (6) shows that the dissipated energy scales quadratically with ε_0 .

The stress response of polymers becomes nonlinear under sufficiently large oscillatory strain or stress amplitudes in tension/tension (ε) as large amplitude oscillatory elongation (LAOE) [1–3]. The deviation from a direct proportionality between the applied strain and the stress response ($\sigma \approx \varepsilon$) is called the nonlinear regime. In this regime, the linear material parameters, such as the storage and loss moduli, become functions of the applied strain amplitude; i.e. $E'(\varepsilon_0)$ and $E''(\varepsilon_0)$ lose their physical meaning as characteristic material parameters [4,5].

For the rheological behavior of soft materials in shear, typically four different types of nonlinear $G'(\gamma_0)$ and $G''(\gamma_0)$ behavior have been reported. Firstly, the so-called strain-thinning occurs when both parameters decrease with increasing strain amplitude. Secondly, strain-hardening occurs when G' and G'' increase with increasing strain amplitude. Thirdly, a weak strain overshoot is obtained when G' decreases but G'' has a maximum before also decreasing. Finally, a strong strain overshoot can be observed when both parameters have a local maximum before decreasing [4]. In dynamic tension/tension, an important $E'(\varepsilon_0)$ increase is less probable due to high damage to the sample, but the two different $E''(\varepsilon_0)$ behavior are expected to occur. But both $E''(\varepsilon_0)$ behaviors are expected to have a different effect on the dissipated energy and the surface temperature as a function of the strain amplitude.

Fourier transform (FT) is a well-known technique to analyze and quantify with high sensitivity nonlinear contributions in the stress waveform using higher harmonics in the Fourier spectra of the time dependent stress [3,6]. For a sufficiently high number of data points in the time domain, the stress can be quantified in the frequency domain using a limited number of frequencies as $I_1(\omega_1)$, $I_2(2\omega_1)$, $I_3(3\omega_1)$, etc., while the remaining points of the spectrum are considered as non-periodic and are associated to noise [7]. As a consequence, the harmonics analysis acts as a very efficient noise filter of the time data, assuming a periodic stress signal: $\sigma(t) = \sigma(t) + T$.

The loading conditions, such as tension/tension [1], or an anisotropy in the sample [8], result in a deformation direction dependence of the stress and the moduli: $\sigma(t) (\varepsilon_+) - \sigma_{mean} \neq -(\sigma(t) (\varepsilon_-) - \sigma_{mean})$ and $E(t) (\varepsilon_+) \neq E(t) (\varepsilon_-)$. This direction dependence can be described by a periodic, nonlinear and asymmetric stress response. In this case, the modulus becomes a function of the applied deformation as $E = E(\varepsilon)$ and a Taylor series expansion of the modulus contains even and odd powers of the strain as [9,10]:

$$E(\varepsilon) = E_0 + E_1 \varepsilon^1 + E_2 \varepsilon^2 + E_3 \varepsilon^3 + \dots \quad (7)$$

Hooke's law can be used to describe the stress response of a simple nonlinear 1D elastic solid body (spring) as:

$$\sigma = E(\varepsilon)\varepsilon \quad (8)$$

Inserting Eq. (2) and Eq. (7) into Eq. (8) gives:

$$\sigma = E_0 \varepsilon + (E_0 + \varepsilon E_1) \varepsilon_0 e^{i\omega_1 t} + (E_1 + \varepsilon E_2) \varepsilon_0^2 e^{2i\omega_1 t} + (E_2 + \varepsilon E_3) \varepsilon_0^3 e^{3i\omega_1 t} + \dots \quad (9)$$

In a more general form, including the phase angles, Eq. (9) can be rewritten as Eq. (10) showing that an asymmetric nonlinear stress response contains even and odd higher harmonics as [2,10,11]:

$$\sigma = \sum_{n=0}^{\infty} I_n e^{in\omega t + \delta_n} \quad (10)$$

The magnitude of the higher harmonics (I_n , $n > 1$) are typically normalized by the fundamental one (I_1) and reported as $I_n/I_1 = I_{n/1}$. For example, the relative third harmonic intensity is presented as $I_{3/1}$.

Furthermore, for an oscillatory deformation in T/T, the asymmetry of the stress response from the loading condition itself needs to be taken into account. The stress response of a material under LAOE is asymmetric ($\sigma(t) - \sigma_{mean} \neq -(\sigma(t + T/2) - \sigma_{mean})$) due to different stress responses during the loading and unloading half cycles; i.e. the oscillatory tension is intrinsically nonlinear from the loading mode; i.e. $\sigma(\varepsilon +) - \sigma_{mean} \neq -(\sigma(\varepsilon -) - \sigma_{mean})$.

In the case of a nonlinear stress response, the first question arising regarding the dissipated energy is if Eq. (6) is still true; i.e. if the area inside the Lissajous curve is still proportional to E'' . As stated in the literature [12,13], neither even ($I_{2/1}$, $I_{4/1}$, etc.) nor odd higher harmonics ($I_{3/1}$, $I_{5/1}$, etc.) contribute to the area of the Lissajous curve due to symmetry reasons. Consequently the dissipated energy only depends on the loss modulus as shown in Appendix A and in Fig. 1 comparing a linear (σ_{lin}), a nonlinear symmetric (σ_{odd}) and an asymmetric nonlinear stress response ($\sigma_{even+odd}$).

Eq. (6) can describe the dissipated energy in the linear regime, but the loss modulus becomes a function of the applied strain amplitude in the nonlinear regime: $E''(\varepsilon_0)$. In this case, W_{diss} also depends on the

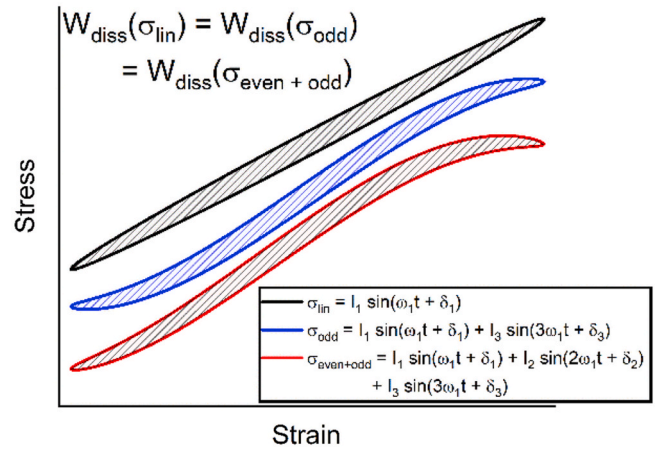


Fig. 1. Lissajous curves of a linear, a symmetric nonlinear and an asymmetric nonlinear stress response. The dashed areas inside the curves is the same for all three curves showing that the area enclosed only depends on the amplitude (I_1) and the phase angle (δ_1) of the fundamental harmonic, which are the same for all three curves ($I_1 = 1$, $\delta_1 = 0.1$) and the area is independent of higher harmonics (for the blue and red curves: $I_2 = 0.1$, $I_3 = 0.1$, $\delta_2 = 0$ and $\delta_3 = 0$). (For interpretation of the references to colour in this figure legend, the reader is referred to the Web version of this article.)

strain amplitude dependence of E'' as:

$$W_{diss} = \pi \varepsilon_0^2 E''(\varepsilon_0) \quad (11)$$

For amorphous polymers like polystyrene (PS), the loss modulus increases with increasing strain amplitude in the nonlinear regime [14], so $E'' \propto \varepsilon_0^n$, with $n > 0$.

During mechanical fatigue in tension/tension, the maximum surface temperature monotonously increases with a small oscillation at the frequency of the strain up to a plateau [15–18] as shown in Fig. 2 for a high density polyethylene (HDPE) sample at $\omega_1/2\pi = 5$ Hz and $\varepsilon_0 = 1.4\%$. This increase of the maximum surface temperature (T_{max} , intrinsic heating) occurs for polymers due to reversible viscous heating or due to irreversible plastic deformation, which occurs beyond yielding for the materials investigated in this article [19–21]. Additionally, for semi-crystalline polymers (polyesters) like polyethylene terephthalate (PET) [22], uniaxial tension beyond yielding can lead to local strain-induced crystallization, generating additional dissipated heat. Typically, T_{max} increases rapidly at the beginning of a fatigue test (transient regime), then levels off to a plateau (steady state regime) and finally increases again at failure. The plateau temperature occurs when an equilibrium between the dissipated energy and heat convection loss is reached, while its value depends on the loss modulus and the applied strain amplitude. In contrast to stress controlled testing, the strain amplitude does not change during strain controlled testing, so the dissipated energy dependence shown in Eq. (11) cannot produce a thermal runaway [23], which is a result of mechanical fatigue and a temperature dependence of the moduli. At first, the mechanical fatigue softens the sample, so the strain amplitude must increase to keep the stress amplitude constant. As the dissipated energy depends on the strain amplitude, the temperature of the sample increases, resulting again in a moduli decrease. Consequently, larger strain amplitudes must be applied to keep the stress constant, which will finally result in a melt-down or failure of the sample at large strain amplitudes.

The surface temperature oscillation (so-called thermoelastic coupling) is an entropy driven process that can be explained by volume increase during the loading half cycle, resulting in a surface temperature decrease, combined with a volume reduction during unloading leading to a temperature increase [24–26]. This phenomenon is a solid-state equivalent of the Joule-Thompson effect. Consequently, the maximum surface temperature decreases when the samples is stretched, while increasing when the samples in compressed or unloaded as:

$$dT = - T_0 \frac{\alpha}{\rho c_p} d\sigma \quad (12)$$

where α is the linear expansion coefficient, ρ is the density and c_p is the heat capacity at constant pressure [27]. For a viscoelastic material in the linear regime, the decreasing surface temperature is associated to the thermoelastic coupling effect and is directly proportional to the applied strain increase and vice-versa which can be written as:

$$T_{max} \propto - \varepsilon \quad (13)$$

For a sinusoidal deformation as described by Eq. (2), the maximum surface temperature can be described by a constant term associated to intrinsic heating and an oscillatory one due to thermoelastic coupling as:

$$T_{max} = T_0 - T_1 \sin(\omega_1 t + \delta_1) \quad (14)$$

The negative sign refers to the fact that T_{max} , due to thermoelastic coupling, has a phase shift of π with respect to the stress, in contrast to the inverse thermoelastic coupling, the so-called Joule-Gough effect, where the temperature changes are in phase with the strain as occurring for rubber-like materials [28]. For polyamide 6, both thermal coupling effects can be detected, depending on the material humidity [29]. The energy balance of thermoelastic coupling over one oscillatory cycle is zero, as the energy gained during the compressive half cycle cancels with the one lost during sample stretching.

The objective of this work is to correlate the thermal response of a material with the mechanical stress response under fatigue in LAOE. Under strain controlled conditions for the linear viscoelastic case, T_{max} should correlate with the linear parameters (loss modulus E'' and complex modulus E^*) using Eqs. (6) and (12). The intrinsic heat, represented by T_0 , is proportional to E'' , while T_1 is associated to E^* . So a complete relation can be written as:

$$T_{max} = T_0(E'') - T_1(E^*) \sin(\omega_1 t + \delta_1) \quad (15)$$

The mechanically irreversibly energy lost corresponds to the intrinsic heat, while the mechanically reversibly stored energy corresponds to thermoelastic coupling, which is a reversible process and the energy gain in the loading cycle (entropy decrease) is lost during the unloading cycle.

If the stress and strain are no longer directly proportional (nonlinear case) and the stress can be described by a series of higher harmonics as shown in Eq. (10), T_{max} also needs to be expanded by a series of higher harmonics as:

$$T_{max} = T_0(E'') - T_1(I_1) \sin(\omega_1 t + \delta_1) - T_2(I_2) \sin(2\omega_1 t + \delta_2) - T_3(I_3) \sin(3\omega_1 t + \delta_3) - \dots \quad (16)$$

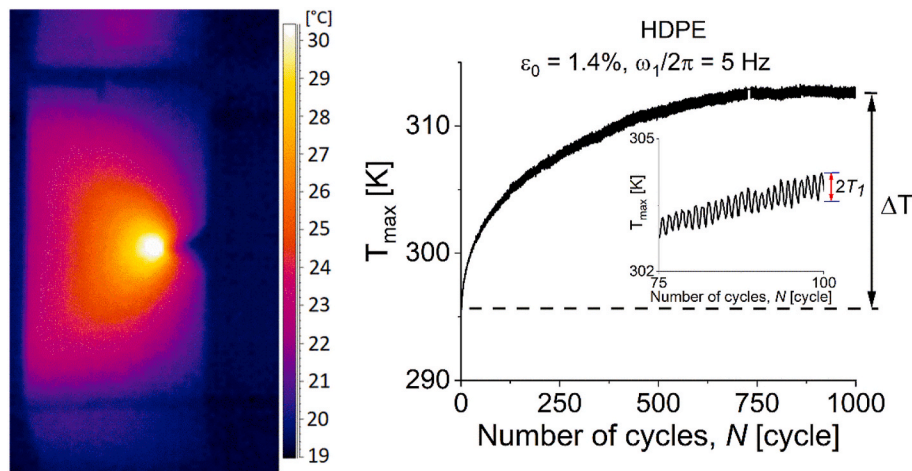


Fig. 2. Thermal image of a HDPE sample clearly showing the highest temperatures at the highest stress concentration (notch tip) and the evolution of T_{max} in the first 1000 cycles for a fatigue test at $\varepsilon_0 = 1.4\%$ and a frequency of $\omega_1/2\pi = 5$ Hz. The temperature rises due to intrinsic heating, but small oscillations (inset) occur due to thermoelastic coupling.

To investigate intrinsic heating and thermoelastic coupling separately, static tension and dynamic deformation controlled fatigue tests at $\omega_1/2\pi = 0.2$ Hz and 5 Hz were performed for six polymers: high density polyethylene (HDPE), low density polyethylene (LDPE), ultra high molecular weight polyethylene (UHMWPE), polyamide 6 (PA6) and two grades of polypropylene (PP); i.e. an injection grade (PP-T) and a rotomolding grade (PP-RX). Firstly, the thermoelastic coupling effect is investigated in static uniaxial tension. Secondly, intrinsic heating is investigated for fatigue tests at $\omega_1/2\pi = 5$ Hz and the temperature increase is correlated with the dissipated energy density calculated from the stress response and the loss modulus respectively, as well as common fatigue prediction concepts based on the surface temperature analysis. Finally, thermoelastic coupling is investigated in dynamic testing via Fourier transform analysis for the fatigue tests at $\omega_1/2\pi = 5$ Hz and for a low frequency ($\omega_1/2\pi = 0.2$ Hz) where plastic deformation is more pronounced and larger strains are accessible without immediate failure.

2. Experimental setup

The static tensile tests at different strain rates ($\dot{\epsilon} = 0.05, 0.1, 0.2, 0.5, 0.75, 1$ and 2 mm/s) and the fatigue tests with a sinusoidal deformation at a frequency of $\omega_1/2\pi = 5$ Hz and 0.2 Hz, a R ratio (the ratio of minimum (ϵ_{\min}) to maximum (ϵ_{\max}) strain) of $R = 0.3$ and a clamp distance of 24 mm were performed on an Acumen 3 (MTS) mechanical testing machine in the strain controlled mode. The time signals for the force and the deformation under dynamic testing were recorded via a custom written LabView program with a sampling rate of 200 points/cycle using oversampling [30]. The nonlinear parameters ($I_{2/1}$ and $I_{3/1}$) were calculated via Fourier transform using a custom written MATLAB script. The tests were performed at room temperature ($RT \approx 23$ °C) and followed by a thermal camera (FLIR ThermoVision A320) recording with a

sampling rate of 35 points/second.

Low density polyethylene (LDPE, LyondellBasell, Petrothene NA202000), high density polyethylene (HDPE, Chevron Phillips Chemical Company, Marlex HHM 5502BN), ultra high molecular weight polyethylene (UHMWPE, Himont), polyamide 6 (Nylon 6 or PA6, Firestone, CLM200-001) and polypropylene (PP, Tairipro, K9017 (PP-T) and Rotoworx, RMPP141, (PP-RX)) were used as typical polymers. The samples were compression molded (180 °C for HDPE and LDPE, 210 °C for UHMWPE, 240 °C for PA6, and 195 °C for PP-T and PP-RT at 2.5 MPa) into a notched rectangular mold (1.3 mm \times 13 mm \times 45 mm, 3 mm notch depth, middle of the length side). A schematic drawing of the sample geometry is shown in Appendix B.

3. Thermal analysis in static tension

Fig. 3 presents the stress, as well as the minimum (T_{\min}) and the maximum (T_{\max}) surface temperature, as a function of the strain during static tensile tests on HDPE, PA6 and PP-T ($\dot{\epsilon} = 0.2$ mm/s). The stress-strain curves have typical behaviors of semi-crystalline materials: a linear regime at low deformation followed by yielding of the sample and then failure after necking, thus plastic deformation. For all the materials investigated, T_{\max} starts to rise when the sample is yielding, but the temperature increases due to plastic deformation while the damage level of each sample differs between the investigated materials: it is more important for PA6, followed by UHMWPE, the PP, LDPE and HDPE [31]. Furthermore, T_{\max} for PA6 starts to oscillate above $\epsilon = 8\%$, which can be related to strain-induced crystallization due to plastic deformation as described in the literature for PET [32].

The minimum surface temperature (T_{\min}) decreases in the linear regime in a tensile test linear with increasing strain, due to thermoelastic coupling as the entropy decreases by stretching the solid sample: more

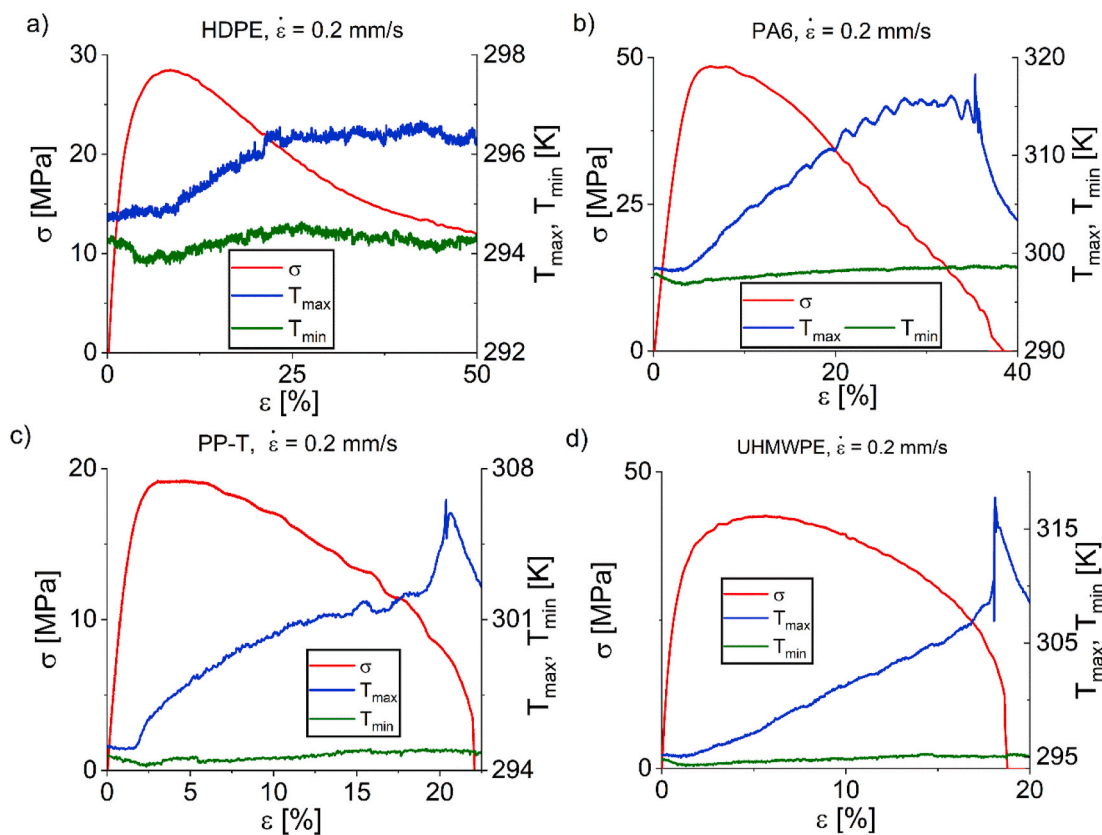


Fig. 3. Stress (σ) and maximum surface temperature (T_{\max}) as a function of strain (ϵ) during a static tensile test of: a) HDPE, b) PA6, c) PP-T and d) UHMWPE at a rate of 0.2 mm/s. The surface temperature of PA6, PP-T and UHMWPE increases when the material yields as the plastic zone is reached, while this only occurs at very large strain amplitudes and is very limited for HDPE.

order is created as the molecules get aligned. Consequently, the direct proportionality as shown in Eq. (12) can be applied for a uniaxial tensile test. As the fatigue tests are performed at different strain rates (constant frequency but different strain amplitudes), the effect of the strain rate on T_{\min} is further investigated. Fig. 4 shows that the time dependent rate of T_{\min} decreases as a function of the applied strain rate revealing a linear correlation between them as:

$$\frac{dT_{\min}}{dt} = -T_e \dot{\epsilon} \quad (17)$$

Equation (17) allows to connect the thermoelastic effect in uniaxial tension with the one in dynamic tension. At a given frequency, the time for each cycle is constant (at 5 Hz it takes 0.1 s per half cycle loading), thus the strain rate increases with increasing strain amplitude. Consequently, the amplitude of the thermoelastic coupling (T_e) is expected to scale linearly with the strain amplitude ($T_e \sim \epsilon_0$).

Furthermore, the different slope (T_e) between the different polymers can be related to the mobility of the polymer chains: the less mobile they are, the larger is T_e . The chain mobility was determined by the loss tangent, $\tan(\delta_1)$, the ratio of loss to storage modulus, at very small strain amplitudes, when material properties are independent of the strain amplitude. The $\tan(\delta_1)$ values are shown in Table 1, decreasing from LDPE ($\tan(\delta_1) = 0.166$) via UHMWPE (0.09), HDPE (0.071), the two PP (0.057 and 0.061) to PA6 (0.033). The thermoelastic effect describes an energy loss due to a decrease in entropy. At a given strain, the less mobile the polymer chains are, the higher the mechanical force is needed to deform the material and squeeze it into a more ordered state. As a consequence, the surface temperature decrease is stronger and T_e is larger. The mobility of the polymer chains mainly depends on the glass transition temperature, T_g ($T_{g,PA6} > T_{g,PP} > T_{g,PE}$), and on the degree of crystallinity X ($X_{HDPE} > X_{UHMWPE} > X_{LDPE}$) so it is expected that $T_e(PA6) = 1.25 > T_e(PP-RX) = 0.83 > T_e(PP-T) = 0.67 > T_e(HDPE) = 0.66 > T_e(UHMWPE) = 0.5 > T_e(LDPE) = 0.25$.

4. Dynamic testing fatigue testing

4.1. Intrinsic dissipated heat

The evolution of the maximum surface temperature and the mechanical parameters (E' , E'' and E_0) is reported in Fig. 5 as a function of

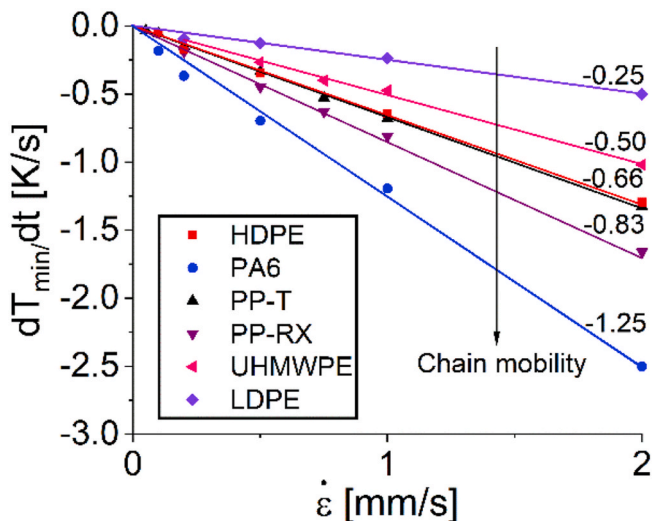


Fig. 4. The rate of temperature decrease due to the thermoelastic effect as a function of the applied strain rate. For the investigated materials (HDPE, PA6, PP-T, PP-RX, UHMWPE and LDPE), a linear correlation between the time dependent rate of change of the minimum surface temperature and the strain rate was found with different slopes.

the number of cycles (N) for: a) HDPE ($\epsilon_0 = 1.4\%$), b) PA6 ($\epsilon_0 = 1.6\%$) and c) PP-T ($\epsilon_0 = 3.2\%$). Storage and loss modulus were calculated via FT of the stress signal and as described in Eqs. (4) and (5). This allows to simultaneously follow the changes, as well as compare the mechanical parameters and the surface temperature response due to ongoing fatigue. For the materials investigated, the surface temperature rapidly increases at the beginning of the test and then levels off to a constant value when a thermal equilibrium state is reached, before decreasing again due to ongoing fatigue and damage accumulation [33]. The E'' trend is of high importance due to its direct proportionality with the dissipated energy and differs between the materials. While E'' monotonously decreases with the cycle number for HDPE and PP-T, it first increases to a plateau value at large strain amplitudes [34], before decreasing close to failure for PA6. For PP-T, the substantial temperature increase during the first cycles can be related to plastic deformation and damage because at $\epsilon_0 = 3.2\%$, the sample is deformed far beyond its yield point ($\epsilon = 3\%$) around resulting in an instantaneous surface temperature increase.

To better understand the relationship between the plateau value of the surface temperature (ΔT) and the dissipated energy calculated from the mechanical stress response, ΔT as well as the dissipated energy density at the beginning of each test ($W_{diss,0}$) and when ΔT reaches a constant value ($W_{diss,p}$) are analyzed as a function of the applied strain amplitude. In Fig. 6a, ΔT is plotted as a function of the applied strain amplitude for the materials investigated. For PP-T, PP-RX, UHMWPE and LDPE, a quadratic relation between ΔT and ϵ_0 can be found for small strain amplitudes, followed by a decrease of the power-law exponent to around 1.1 for PP-T, PP-RX and LDPE, while it increases to about 3 for UHMWPE at very large strain amplitudes. For HDPE and PA6, ΔT follows a power-law relationship with an exponent around 2.7, but ΔT rapidly increases for PA6 at larger strain amplitudes ($\epsilon_0 > 1-1.2\%$). This important surface temperature rise can be associated with plastic deformation [35].

In Fig. 6b), the dissipated energy density at the beginning of each test ($W_{diss,0}$) and at the ΔT plateau value ($W_{diss,p}$) are plotted as a function of the applied strain amplitude. For the materials investigated, $W_{diss,0}$ and $W_{diss,p}$ are similar at small strain amplitudes and increase quadratically with ϵ_0 . In this regime, the materials behave as linear viscoelastic and E'' is independent of the applied strain amplitude. At larger strain amplitudes, $W_{diss,0}$ is typically larger than $W_{diss,p}$, but the exponent of the $W_{diss,0}$ and $W_{diss,p}$ relation as a function of ϵ_0 changes. It increases to 2.3, 2.5 and 3.0 for HDPE, PA6 and UHMWPE respectively, but decreases to 1.1 for both PP and LDPE. For PA6, a third regime at very large strain amplitudes ($\epsilon_0 > 1\%$) is observed when plastic deformation dominates the damage process, resulting in larger $W_{diss,p}$ than $W_{diss,0}$ values and the exponent of the $W_{diss,p}$ vs. ϵ_0 relation increases to 3.4.

As derived in Eq. (11) for linear viscoelastic materials, such as polymers at small strain amplitudes, the dissipated energy is expected to scale quadratically with ϵ_0 . As ΔT is proportional to $W_{diss,p}$, the quadratic ($n = 2$) increase of ΔT vs. ϵ_0 is as expected for a viscoelastic material in the linear viscoelastic regime leading to:

$$\Delta T \propto \epsilon_0^2 \quad (18)$$

At larger strain amplitudes, the material response gets nonlinear; i.e. E'' becomes a function of ϵ_0 (Eq. (19)) with $n \neq 0$ and consequently the power-law exponent (n) changes.

$$E''(\epsilon_0) \propto \epsilon_0^n \quad (19)$$

The maximum surface temperature increase is related to the dissipated energy density in the equilibrium state (Eq. (20)). As a consequence, the strain amplitude dependence of both the dissipated energy density ($W_{diss,p}$) and the surface temperature increase (ΔT) should have similar exponents which is expected to scale as $2 + n$ for the nonlinear case to give:

$$W_{diss,p} \propto \Delta T \quad (20)$$

Table 1

Strain amplitudes from the Wöhler curves when the fatigue limit is reached ($N_f = 10^6$ cycles), as well as the strain amplitudes when the slopes of the ΔT vs. ε_0 and $W_{diss,p}$ vs. ε_0 correlations change. The elastic and loss moduli (E' and E'') and the $\tan(\delta_1)$ in the linear regime are also reported.

Polymer	ε_0 for $N_f = 10^6$ cycles	Strain amplitude of the deviation of $\Delta T \propto \varepsilon_0^2$	Strain amplitude of the deviation of $W_{diss,p} \propto \varepsilon_0^2$	E' at small ε_0 [MPa]	E'' at small ε_0 [MPa]	$\tan(\delta_1)$ at small ε_0
HDPE	0.24	–	0.24	2100	150	0.071
LDPE	0.36	2.38	2.50	420	70	0.166
UHMWPE	1.38	2.38	2.77	1450	130	0.090
PA6	0.18	–	0.32	1500	50	0.033
PP-T	1.18	1.18	1.18	1600	90	0.057
PP-RX	1.38	1.38	1.38	1800	110	0.061

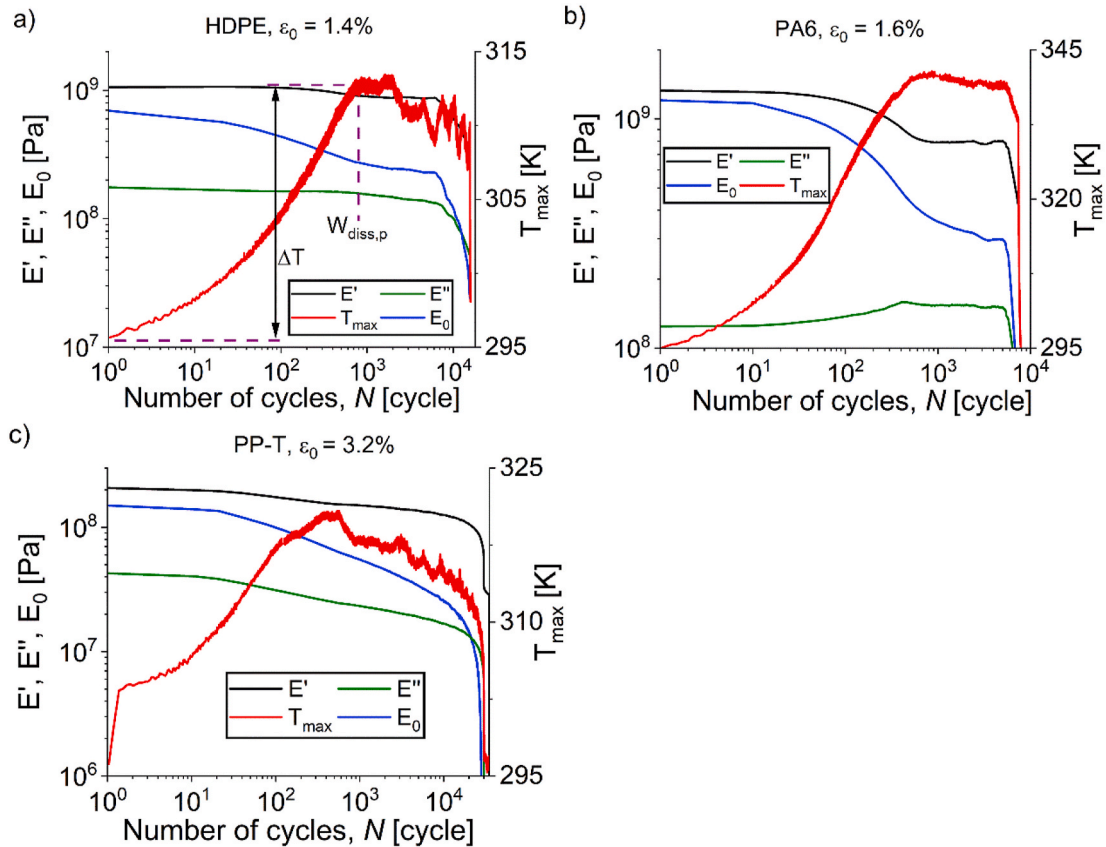


Fig. 5. Typical curves for the mechanical parameters (E' , E'' and E_0) and the maximum surface temperature (T_{max}) as a function of the cycle number (N) for: a) HDPE ($\varepsilon_0 = 1.4\%$), b) PA6 ($\varepsilon_0 = 1.6\%$) and c) PP-T ($\varepsilon_0 = 3.2\%$). An example on how ΔT and $W_{diss,p}$ are calculated is presented in a).

$$W_{diss,p} \propto \varepsilon_0^{2+n} \quad (21)$$

$$\Delta T \propto \varepsilon_0^{2+n} \quad (22)$$

During oscillatory deformation, the total viscous and plastic dissipated energy is proportional to the area enclosed by the hysteresis loop, which is related to the loss modulus. As seen in Fig. 3 for the static tensile tests, PA6 dissipates energy when plastically deformed. For PA6 at $\varepsilon_0 > 1\%$, E' increases at the beginning of the test to a maximum which can be related to plastic deformation and strain-induced crystallization resulting in additional energy dissipation. Consequently, the exponent of the $W_{diss,0}$ and $W_{diss,p}$ vs. ε_0 relation further increases for PA6 at $\varepsilon_0 > 1\%$. This is an interesting finding as plastic deformation is expected to change the shape of the hysteresis loop. However, the dissipated energy is still only related to the area enclosed which is directly proportional to the loss modulus.

It is important to emphasize again that the deviation from the quadratic strain amplitude dependence of the dissipated energy is a

nonlinear phenomena, but only in the sense that E'' is a function of the applied strain amplitude ($E''(\varepsilon_0)$) and is not a characteristic material parameter anymore, not in the sense that a nonlinear stress waveform is necessary ($\sigma \approx \varepsilon$).

4.2. Correlation of the dissipated energy with the wöhler curve

Common concepts to estimate the fatigue properties (Wöhler curve of a material) of metals [36,37], polymers [15], rubbers [38,39] or epoxies [40] correlate the plateau value of the surface temperature (ΔT) with the fatigue lifetime (N_f). Therefore, a series of short oscillatory (stress or strain controlled) tests at different loading or deformation level are performed. The length of each step must be long enough for the surface temperature to reach equilibrium, but also short enough to avoid permanent damage of the sample. Only the last loading step at large deformation is run to failure to get the fatigue life at the applied strain amplitude. To construct a Wöhler curve, a second point is needed which is obtained by the assumption that the fatigue limit is reached when the

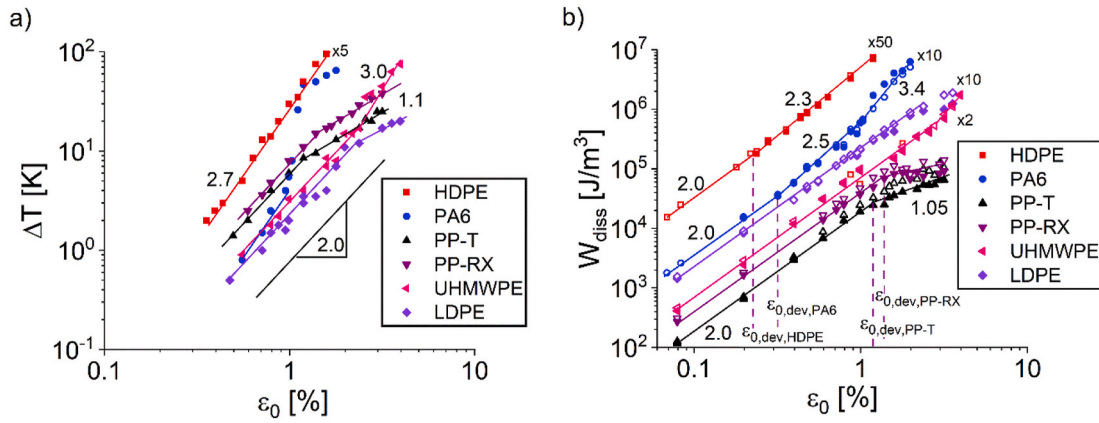


Fig. 6. a) The plateau value of the temperature rise (ΔT) and b) the dissipated energy density (W_{diss}) as a function of the strain amplitude. The closed symbols represent the ΔT and W_{diss} in the thermal plateau regime, while the open symbols in b) represent the value of W_{diss} at the beginning of the test. The lines are guides to the eye with their respective slope as indicated.

material behaves completely linear; i.e. for metals no heat is dissipated due to plastic effects and that polymers behave linear viscoelastic. The onset of a nonlinear behavior will result in a change in the measured surface temperature; i.e. in the ΔT vs. ε_0 relation as discussed in section 4.1 and is typically correlated with a fatigue lifetime of 10^6 cycles as the fatigue limit [38]. This method was originally established for metals with the assumption that without plastic deformation, which results in the dissipation of energy, no failure would occur. As both parameters (ΔT and N_f) depend on the applied strain amplitude, a power-law dependence between ΔT and N_f was empirically found as [15,41]:

$$\Delta T N_f^{b_T} = C_T \quad (23)$$

where b_T and C_T are material parameters.

Since the temperature rise to reach the thermal equilibrium (ΔT) correlates with the plateau value of the dissipated energy ($W_{diss,p}$), Eq. (23) should be rewritten as:

$$W_{diss,p} N_f^{b_W} = C_W \quad (24)$$

This raises the question if this prediction also works for the polymers investigated via ΔT and $W_{diss,p}$, as well as which parameter better predicts the fatigue limit of the Wöhler curves.

Fig. 7 presents the Wöhler curves of the six materials investigated which allows to extract the strain amplitudes at failure after 10^6 cycles

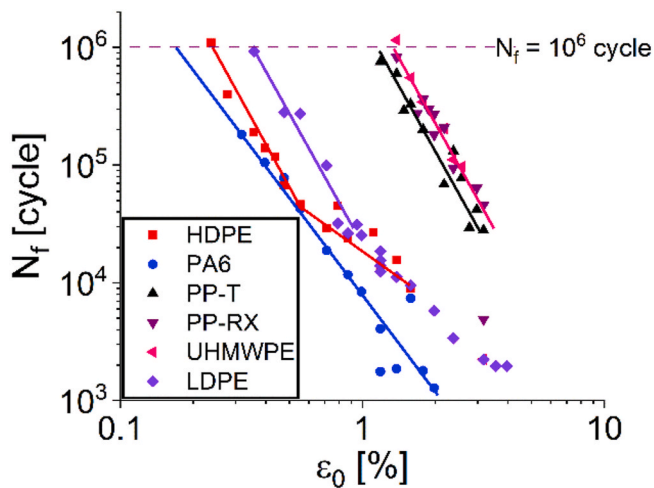


Fig. 7. The Wöhler curves of the investigated HDPE, PA6, PP-T, PP-RX, UHMWPE and LDPE. The dashed line marks failure after 10^6 cycles ($N_f = 10^6$ cycles).

($\varepsilon_{0, \text{Polymer}, 10^6}$). The values are listed in Table 1 together with the strain amplitudes related to the transition in the ΔT vs. ε_0 and the $W_{diss,p}$ vs. ε_0 correlations.

As seen in Fig. 6 and Table 1, a change in the ΔT vs. ε_0 dependence can only be detected for PP-T, PP-RX, UHMWPE and LDPE, but for UHMWPE and LDPE it occurs at very large strain amplitudes already in the low cycle fatigue regime. For HDPE and PA6, no regime with $n = 2$ can be detected as it would be below 1 K, which is at the experimental detection limit. Nevertheless, the dissipated energy density can be calculated for much smaller strain amplitudes, so a change in the trend from a quadratic ($W_{diss,p} \propto \varepsilon_0^2$) to a non-quadratic behavior ($W_{diss,p} \propto \varepsilon_0^{2+n}$) can be detected for all the materials investigated. The best prediction via both methods is for both PP, showing clear changes in the ΔT vs. ε_0 and the $W_{diss,p}$ vs. ε_0 relation around $\varepsilon_0 = 1.2\%$, which fits well with the expected strain amplitude for failure after 10^6 cycles (Table 1). For HDPE, the change in the slope of the $W_{diss,p}$ vs. ε_0 relation is very limited, from 2.0 to around 2.3, so the strain amplitude when this change occurs is prone to errors but cannot be predicted via ΔT , while no change can be detected before very large strain amplitudes are reached for UHMWPE and LDPE. For PA6, the prediction via ΔT does not work either, while the one via $W_{diss,p}$ predicts the strain amplitude of $N_f = 10^6$ with a deviation of 0.2% in strain amplitude, which still gives a good approximation about the Wöhler curve.

Another critical parameter to compare both approaches, via the surface temperature and the calculated dissipated energy from the mechanical material response, is the measurement sensitivity. This is especially of interest, as for all materials, independent of the underlying material behavior generating heat dissipation and the physical interpretation of the phase angle, the dissipated heat can be described by the area enclosed by the hysteresis loop, which can be calculated via Eq. (11). Surface temperature analysis is a way to determine the deviation from the linear behavior, as it can also be directly extracted from the stress. Therefore, the mechanical testing device needs to be sufficiently precise in terms of: (I) strain resolution, (II) sensitivity of the force transducer, (III) the signal recording and (IV) the analysis of the stress needs to be done carefully. For example, oversampling [30], a high sampling rate and Fourier transform analysis should be used so that even small phase angle δ_1 can be precisely quantified with high reproducibility. This allows to determine the dissipated energy with high reproducibility at much smaller strain amplitudes than the surface temperature analysis.

4.3. Thermoelastic coupling and T_{max}

4.3.1. Fatigue tests at $\omega_1/2\pi = 5$ Hz

To quantify the thermoelastic coupling effect, the time signal of the

maximum surface temperature was analyzed via Fourier transform. For the fatigue tests at a frequency of $\omega_1/2\pi = 5$ Hz, the first 50 cycles after reaching the plateau were analyzed. The amplitude of the thermoelastic effect is called T_1 :

$$T_{max} = T_0 - T_1 \sin(\omega_1 t + \delta_1) \quad (25)$$

In Fig. 8a, a Fourier spectrum of T_{max} for PA6 at $\epsilon_0 = 1.6\%$ and $\omega_1/2\pi = 5$ Hz is shown, T_0 at $\omega_1/2\pi = 0$ Hz and T_1 at $\omega_1/2\pi = 5$ Hz can be seen clearly. In Fig. 8b), the amplitude T_1 of the thermoelastic coupling is presented normalized with $\epsilon_0 (T_1/\epsilon_0)$ as a function of the applied strain amplitude. At small amplitudes, T_1/ϵ_0 is constant, so T_1 scales linearly with ϵ_0 (Eq. (26)) for the investigated materials, but deviates from this behavior at large strain amplitudes. As reported in section 3, the surface temperature decrease due to thermoelastic coupling is directly proportional to the strain rate. At a constant frequency, the strain rate is directly proportional to the applied strain amplitude. Therefore T_1/ϵ_0 is expected to be constant as:

$$\frac{T_1}{\epsilon_0} = T_D = const. \quad (26)$$

In Fig. 8b), the trend of T_D of Eq. (26) is similar to the one of T_S for the static tensile tests in Fig. 4: the lower the chain mobility, the more pronounced is the thermoelastic coupling and consequently the higher is T_1/ϵ_0 at small strain amplitudes.

At large strain amplitudes, T_1/ϵ_0 decreases for PA6, PP-T, PP-RX, HDPE and LDPE, while it further increases for UHMWPE. For UHMWPE, the transition from a linear to a nonlinear T_D behavior occurs at the same strain amplitude as the change of the ΔT vs. ϵ_0 behavior due to nonlinear viscoelasticity and plasticity. As shown in Eq. (12), T_1 is directly

proportional to the stress, so when the stress vs. strain relationship becomes nonlinear, $T_D(\epsilon_0)$ should also become nonlinear. Furthermore, changes of the quadratic ΔT vs. ϵ_0 relationship correlate with the nonlinear $E''(\epsilon_0)$ behavior, for $T_1(\epsilon_0)$ the nonlinear $E^*(\epsilon_0)$ behavior needs to be considered, as shown in Eq. (16). The onset of a nonlinear elastic stress response can simply be determined by $E^*(\epsilon_0)$ under strain controlled conditions. In Fig. 8c), E^* is presented as a function of ϵ_0 . To avoid the influence of cumulative plastic strains, each datapoint represents one experiment and sample. For all the materials, $E^*(\epsilon_0)$ is constant at small strain amplitudes and decreases rapidly in the nonlinear regime at large strain amplitudes due to viscoelastic nonlinearity, plastic deformation and damage. The open symbols represent the $E^*(\epsilon_0)$ values at the beginning of the test, the closed ones after the T_{max} plateau was reached, where T_1 is also calculated. For UHMWPE, $E^*(\epsilon_0)$ presents a second plateau in the $\epsilon_0 = 2-4\%$ range. For both PP, HDPE and PA6, T_D levels off at large strain amplitudes, as expected also from the $E^*(\epsilon_0)$ decrease, but $T_D(\epsilon_0)$ of LDPE is not influenced by the $E^*(\epsilon_0)$ decrease and even increase for UHMWPE, which might only correlate with the second $E^*(\epsilon_0)$ plateau at large ϵ_0 .

As especially the nonlinear T_D behavior of UHMWPE does not correlate with the nonlinear $E^*(\epsilon_0)$ behavior, the direct proportionality with the stress is no longer valid, and the substantial $T_D(\epsilon_0)$ increase must correlate with plastic deformation and damage of the UHMWPE samples at large strain amplitudes [42].

4.3.2. Fatigue tests at $\omega_1/2\pi = 0.2$ Hz

To further investigate the thermoelastic coupling and to detect possible nonlinear contributions in T_{max} , tests at a much lower frequency

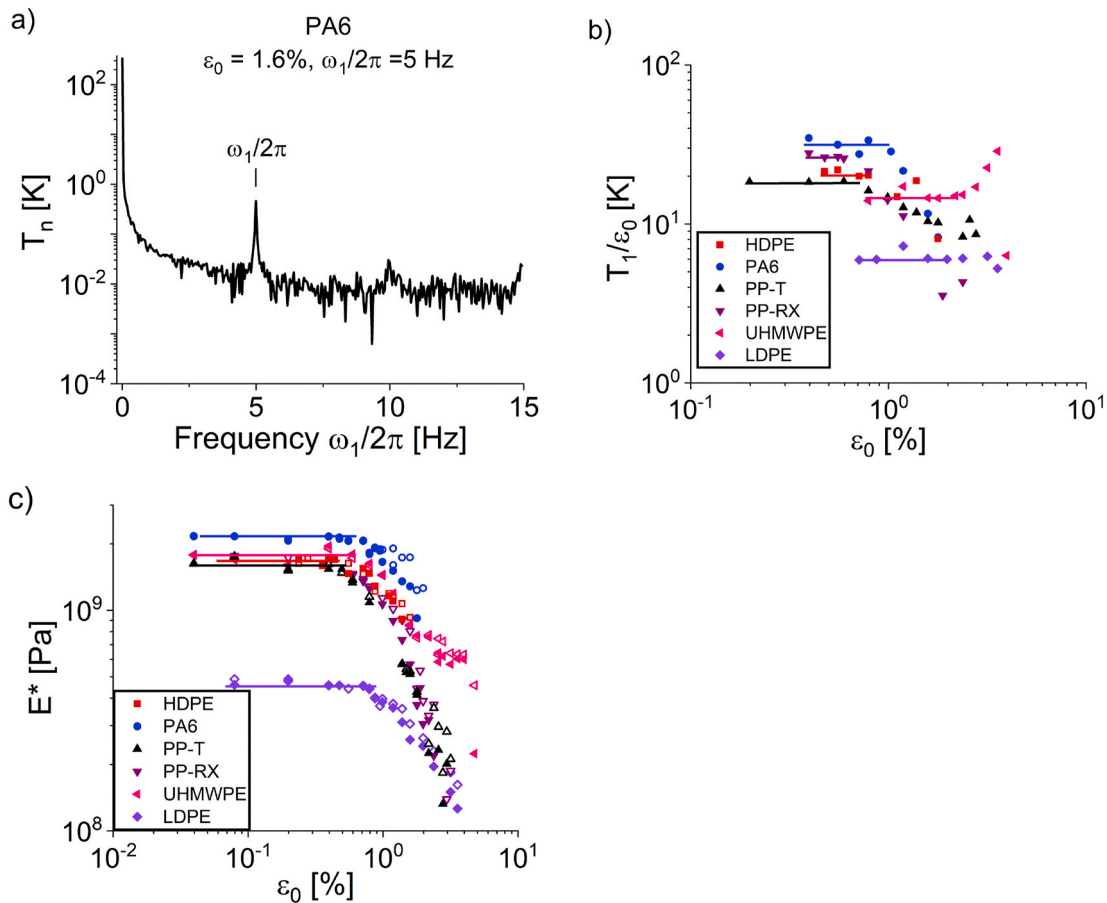


Fig. 8. a) T_{max} Fourier spectrum of PA6 at $\epsilon_0 = 1.6\%$ for the first 50 cycles after reaching the T_{max} plateau. b) The amplitude of the thermoelastic coupling (T_1) normalized by the deformation amplitude (T_1/ϵ_0) as a function of the applied strain amplitude. c) The complex modulus $E^*(\epsilon_0)$ at the beginning of the test (open symbols) and after reaching the plateau value of T_{max} (closed symbols).

($\omega_1/2\pi = 0.2$ Hz) were performed to increase the number of data points per cycle and to improve the signal to noise ratio of the FT spectra. Additionally, this allows to access even larger strain amplitudes as the elongation at break typically increases with decreasing strain rate. Of special interest is the nonlinear regime T_1 , where T_1 increases fast (Fig. 8b) and to investigate if T_{\max} is no longer directly proportional to the strain ($T_{\max} \approx \epsilon$).

Fig. 9 shows the strain, force and maximum surface temperature during the first seven cycles of a fatigue test of PA6 and UHMWPE at $\epsilon_0 = 3.2\%$ and $\epsilon_0 = 7.1\%$, respectively. The stress signal shows that plastic deformation occurs during the first loading half cycle, resulting in a stress maximum before the strain maximum is reached. The maximum surface temperature firstly decreases at the beginning of the test due to thermoelastic coupling, then substantially increases. As shown in Fig. 3 for a static tensile test, PA6 and UHMWPE dissipate energy as heat under plastic deformation, explaining the first substantial temperature rise.

After the first cycle, the surface temperature has two maxima/minima during one strain cycle with different amplitudes, pointing at different physical reason. The peak during the unloading half cycle can be explained by thermoelastic coupling (entropic effects), while the one during the loading half cycle by plastic deformation as PA6 and UHMWPE dissipate energy when deformed beyond yielding; i.e. when plastic deformation occurs as shown in section 3 during static tensile tests. The first peak is fading away with time for PA6 and gets smaller for UHMWPE, as the new plastic deformation decreases with each cycle, accumulating as a permanent stretching of the sample similar to creep.

To quantify the plastic deformation, the time signal of the maximum surface temperature was analyzed via Fourier transform. To describe two maxima during one deformation cycle, T_{\max} needs to contain terms at multiple frequencies of the deformation frequency in the form of:

$$T_{\max} = T_0 - T_1 \sin(\omega_1 t + \delta_1) - T_2 \sin(2\omega_1 t + \delta_2) - T_3 \sin(3\omega_1 t + \delta_3) - \dots \quad (27)$$

An oscillation of the surface temperature with the amplitude of T_1 can be expected from thermoelastic coupling, while T_2 , T_3 , etc. can be related to plastic deformation. In Fig. 10 presents the time evolution of T_{\max} and the FT spectra of cycles 2–6 for PA6 at $\epsilon_0 = 3.2\%$ and UHMWPE at $\epsilon_0 = 7.1\%$, both at $\omega_1/2\pi = 0.2$ Hz. In both cases, a large peak in T_{\max} during the first cycle can be seen, followed by two peaks during one strain cycle for the other first cycles. The Fourier spectra contain, beside the fundamental harmonic at $\omega_1/2\pi = 0.2$ Hz, higher order peaks at $2\omega_1/2\pi = 0.4$ Hz, $3\omega_1/2\pi = 0.6$ Hz, etc.

In Fig. 11, the strain amplitude dependence of T_1 , T_2 and T_3 during cycles 2–6 is presented for PA6 and UHMWPE. As reported in Fig. 8, the Fourier coefficient T_1 scales linearly with the strain amplitude and can be detected under the testing conditions (small strain amplitudes: $\epsilon_0 < 0.2\%$), but levels off around $\epsilon_0 = 1.2\%$ for PA6 and 3% for UHMWPE.

Furthermore, around $\epsilon_0 = 0.8\%$ for PA6 and 1% for UHMWPE, the second harmonic (T_2) starts to appear and rises above the noise level scaling quadratically with ϵ_0 . For UHMWPE around $\epsilon_0 = 3\%$, T_2 gets larger than T_1 . At even larger strain amplitudes, T_3 increases for both materials above the noise level and scales cubically with ϵ_0 . This shows that Fourier transform of T_{\max} is a powerful tool to detect, follow and quantify deviations from a purely sinusoidal behavior of T_{\max} , which can be related to plastic deformation for the polymers investigated. In the literature, temperature variations at twice the fundamental frequency have been described and correlated to plastic deformation for metals such as steel [43].

At large strain amplitudes, the other materials investigated (HDPE, LDPE, PP-T and PP-RX) also show a peak in the surface temperature during the first loading half cycle due to plastic deformation. Afterwards, nonlinear T_{\max} behavior can be detected for all four materials at large strain amplitudes, but T_2 does not typically reach the same level as T_1 and only for LDPE two maxima in T_{\max} can be detected during cycle 2 and 3 at very large strain amplitudes. For example, the waveform of the nonlinear T_{\max} response for PP-T is typically closer to an inverted half wave reflected sine wave.

In Fig. 10a) for PA6, during one strain cycle, T_{\max} has two maxima at the beginning of the test, which reduces to only one at higher cycle numbers; i.e. only the maximum during the unloading cycle caused by thermoelastic coupling remains, while the one during the loading half cycle due to plastic deformation vanishes. In contrast, the second maximum during one strain cycle does not fade away for UHMWPE; only the one during the loading half cycle gets smaller. As UHMWPE is not a rubbery material, inverse thermoelastic coupling is not expected to occur and to cause heat dissipation during the loading cycle. Instead, the heat dissipation during loading can be explained by deformations beyond the yielding point during each cycle. The stress response of UHMWPE during the whole test has its maximum before the strain maximum; i.e. the material yields during each cycle before the maximum deformation is reached.

4.3.3. Correlation between the thermal and mechanical stress response higher harmonics: T_n vs. $I_{n/1}$

Fig. 12a) shows the evolution of the linear and nonlinear mechanical parameters, as well as in Fig. 12b) the Fourier coefficients of the surface temperature, with ongoing fatigue for PA6 at $\epsilon_0 = 3.2\%$ and $\omega_1/2\pi = 0.2$ Hz as presented in Fig. 9a). The mechanical response was decomposed via Fourier transform (Eq. (10)) giving the linear parameters (E' , E'' and E_0), as well as the nonlinear parameters ($I_{2/1}$ and $I_{3/1}$). The linear mechanical parameters show that, from the beginning of the test, the elastic modulus is larger than the average stress ($E' > E_0$). As the tests were performed in strain controlled tension/tension, this means that the sample is instantaneously plastically deformed and is under compression

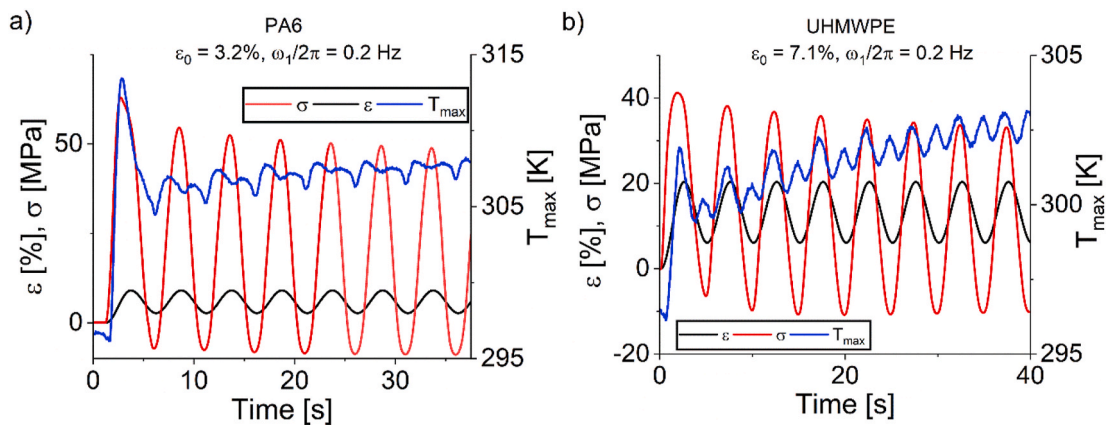


Fig. 9. Strain (ϵ), stress (σ) and maximum temperature (T_{\max}) as a function of time at $\omega_1/2\pi = 0.2$ Hz for: a) PA6 at $\epsilon_0 = 3.2\%$ and b) UHMWPE at $\epsilon_0 = 7.1\%$. After the initial cycle, T_{\max} clearly reveals two maxima during one deformation cycle.

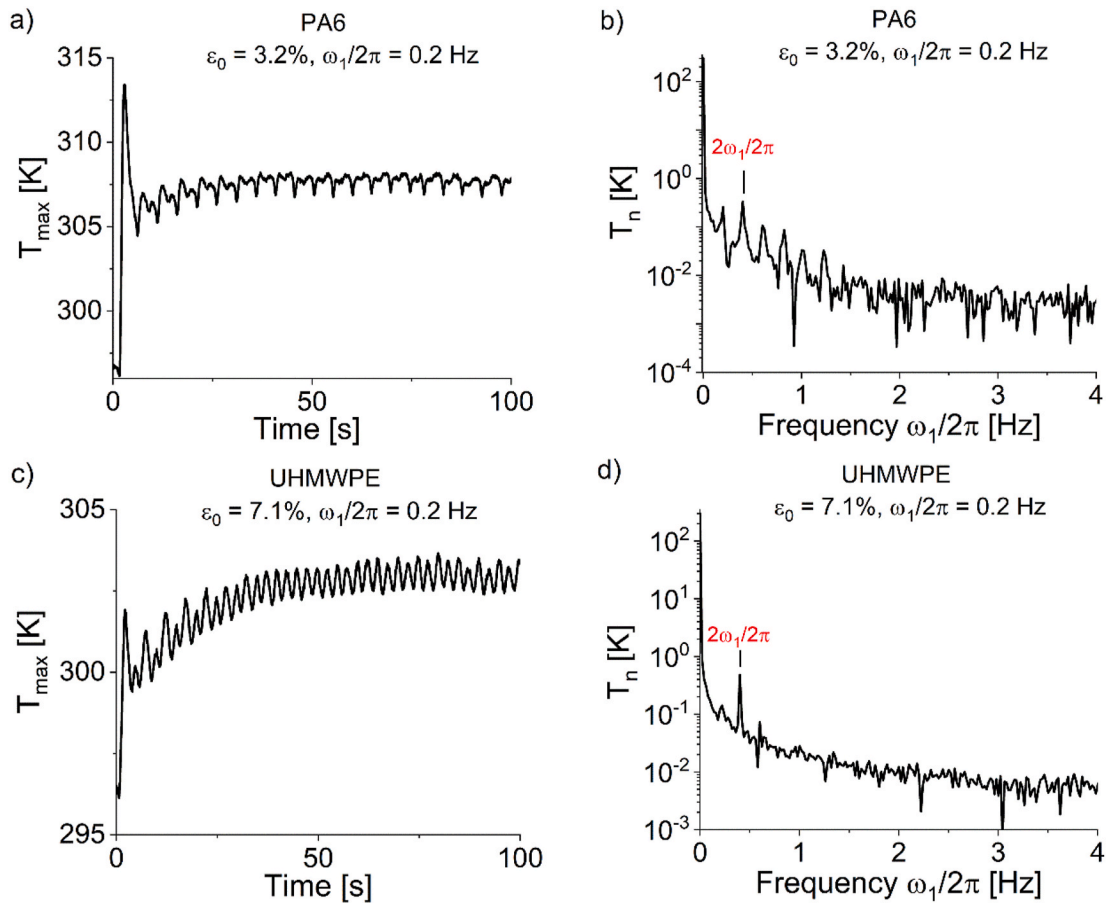


Fig. 10. The evolution of the maximum temperature (T_{max}) during the first 20 cycles (100 s) and the FT spectrum of the first 5 cycles (25 s) after the sharp temperature rise of the initial cycle in a) and b) for PA6 at $\epsilon_0 = 3.2\%$ and $\omega_1/2\pi = 0.2$ Hz, as well as in c) and d) for UHMWPE at $\epsilon_0 = 7.1\%$ and $\omega_1/2\pi = 0.2$ Hz.

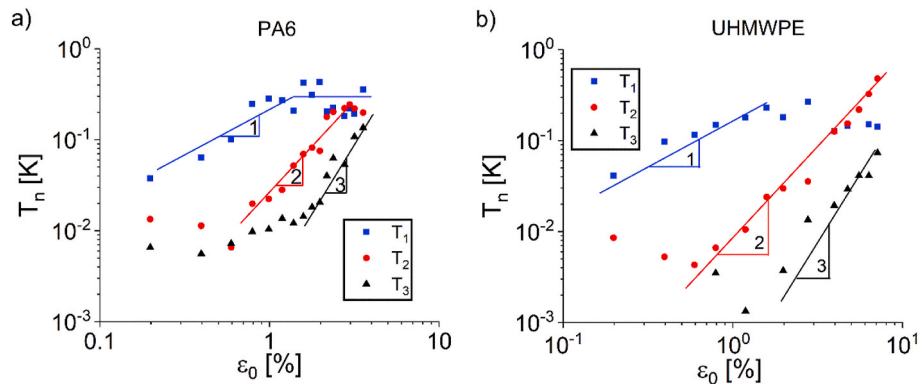


Fig. 11. The temperature fundamental harmonic (T_1), as well as the higher harmonics (T_2 and T_3) as a function of the applied strain amplitude (ϵ_0) for: a) PA6 and b) UHMWPE.

at the strain minimum, resulting in higher level of asymmetry in the stress. This is why $I_{2/1}$ increases rapidly at the beginning of the test, by about a factor of 2.5 within the first 20 cycles, acting as a strong nonlinear fingerprint for plastic deformation.

Due to plastic deformation at the beginning of the test, the Fourier coefficients of the maximum surface temperature (T_{max}) reveal characteristic fingerprints: while T_1 is constant as a first approximation until failure at around $T_1 = 0.23$, T_2 is larger than T_1 at the beginning of the test and decreases from $T_2 = 0.33$ until $N = 25$ to the noise level where T_2 scatters around a constant value of about $T_2 = 0.07$. Fig. 12b) shows that a typical fingerprint in T_{max} can be found during the first 25 cycles

due to plastic deformation, while plastic deformation results in an $I_{2/1}$ intensity increase of the mechanical stress response leaving a permanent fingerprint in the stress as shown in Fig. 12a.

5. Conclusion

The surface temperature evolution during mechanical fatigue testing of high density polyethylene (HDPE), low density polyethylene (LDPE), ultra high molecular weight polyethylene (UHMWPE), polyamide 6 (PA6) and two grades of polypropylene (PP) under large amplitude oscillatory elongation (LAOE) was investigated and correlated with the

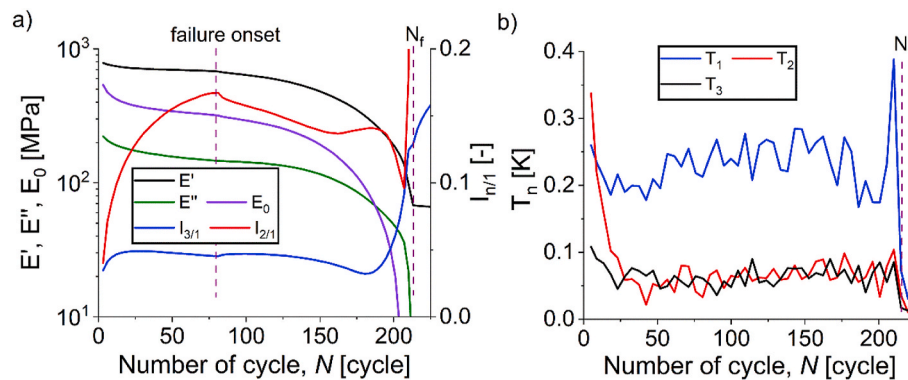


Fig. 12. a) The linear and nonlinear mechanical parameters and b) the Fourier coefficients of the maximum surface temperature for PA6 at $\varepsilon_0 = 3.2\%$ and $\omega_1/2\pi = 0.2$.

mechanical stress response. Firstly, intrinsic heating, associated with viscous and plastic dissipation, and secondly thermoelastic coupling (an oscillation of the surface temperature at the frequency of the deformation) was observed.

Intrinsic heating was correlated with the dissipated energy density, calculated from the mechanical stress response via Fourier transform analysis. During a fatigue test, the surface temperature increased to a plateau value, with the difference ΔT , representing an equilibrium state between the dissipated energy from the mechanical deformation and the heat transfer to the environment (convection loss). A power-law correlation between ΔT and the applied strain amplitude (ε_0) was found for the six materials investigated. The dissipated energy density at the plateau value of the surface temperature ($W_{diss,p}$), calculated from the mechanical stress response, scaled quadratically with ε_0 at small strain amplitudes as expected for a viscoelastic material in the linear regime ($W_{diss,p} \propto \varepsilon_0^2$), before the power-law exponent changed to values close to the ΔT vs. ε_0 correlation at larger strain amplitudes due to nonlinear viscoelastic effects ($W_{diss,p} \propto \varepsilon_0^{2+n}$). Common concepts to rapidly estimate a Wöhler curve via surface temperature analysis was proposed by assuming the fatigue limit ($N_f = 10^6$ cycles) to occur when the ΔT vs. ε_0 deviates from a linear material behavior and increases rapidly. This concept was found to hold only for both PP, but a deviation of the quadratic behavior with ε_0 was observed for the dissipated energy density of HDPE, LDPE, UHMWPE and PA6, all correlating well with the strain amplitude at the onset of the fatigue limit. While ΔT below 1 K were difficult to determine (thermal sensor), $W_{diss,p}$ can be calculated even for very small strain amplitudes only limited by the sensitivity of the testing device (mechanical sensor), underlining the advantage of the calculated dissipated energy density from the mechanical stress over the surface temperature analysis.

Thermoelastic coupling was investigated in uniaxial tension revealing a linear correlation between the applied strain rate and the rate of temperature decrease. In dynamic fatigue testing at $\omega_1/2\pi = 0.2$ Hz and 5 Hz, the surface temperature oscillation was analyzed via Fourier transform showing a direct proportionality of the surface temperature oscillation amplitude with ε_0 ($T_1/\varepsilon_0 = \text{constant}$) at small strain amplitudes, while T_1/ε_0 decreased at large strain amplitudes with a similar trend as $E^*(\varepsilon_0)$ for the materials investigated. This allowed to conclude that T_{\max} in dynamic tension/tension depends on the loss modulus (E'') and the complex modulus (E^*) describing intrinsic heat and thermoelastic coupling, respectively.

At low frequencies and large strain amplitudes, additional higher harmonics at two and three times the fundamental frequency in T_{\max} (T_2 and T_3) were detected in a FT spectrum for the first cycles (about 5) of each test for PA6 and UHMWPE. These higher harmonics occurred when the sample was plastically deformed and heat was additionally dissipated during the loading half cycle. This effect faded away when no more plastic deformation occurred. The second and third higher

harmonics were found to scale quadratically and cubically with ε_0 ($T_2 \propto \varepsilon_0^2$, $T_3 \propto \varepsilon_0^3$), respectively.

Finally, from the results obtained, the correlation and advantages of the calculated dissipated energy density over the surface temperature analysis was shown, as well as the advantages of Fourier transform analysis of the surface temperature oscillation to detect nonlinear fingerprints related to plasticity. These concepts are expected to be valid in general and not only restricted to the materials studied as the concepts used are mathematically/physically sound and are expected to hold for any material.

CRediT authorship contribution statement

Valerian Hirschberg: Formal analysis, Investigation, Methodology, Writing - original draft. **Manfred Wilhelm:** Conceptualization, Supervision, Validation, Writing - review & editing. **Denis Rodrigue:** Conceptualization, Data curation, Funding acquisition, Methodology, Project administration, Resources, Supervision, Validation, Writing - review & editing.

Declaration of competing interest

The authors declare that they have no known competing financial interests or personal relationships that could have appeared to influence the work reported in this paper.

Acknowledgement

The authors acknowledge the financial support of the Natural Sciences and Engineering Research Council of Canada (NSERC) and the much-appreciated technical support of Mr. Yann Giroux (Université Laval).

Appendix C. Supplementary data

Supplementary data to this article can be found online at <https://doi.org/10.1016/j.polymertesting.2021.107070>.

Appendix A

Mathematical derivation of the dissipated energy density in Eqs. (6) and (11).

Appendix B

Schematic drawing of the employed sample geometry.

Funding sources

This research did not receive any specific grant from funding agencies in the public, commercial, or not-for-profit sectors.

Data availability

The raw/processed data required to reproduce these findings cannot be shared at this time as the data also forms part of an ongoing study.

References

- C. Dessi, D. Vlassopoulos, A.J. Giacomini, C. Saengow, *Elastomers in Oscillatory Uniaxial Extension*, 2016.
- A. Giacomini, R. Bird, C. Aumtate, A. Mertz, A. Schmalzer, A. Mix, Viscous heating in large-amplitude oscillatory shear flow, *Phys. Fluids* 24 (2012) 103101, <https://doi.org/10.1063/1.4752777>.
- K. Hyun, M. Wilhelm, C.O. Klein, K.S. Cho, J.G. Nam, K.H. Ahn, S.J. Lee, R. H. Ewoldt, G.H. McKinley, A review of nonlinear oscillatory shear tests: analysis and application of large amplitude oscillatory shear (Laos), *Prog. Polym. Sci.* 36 (2011) 1697–1753, <https://doi.org/10.1016/j.progpolymsci.2011.02.002>.
- K. Hyun, S.H. Kim, K.H. Ahn, S.J. Lee, Large amplitude oscillatory shear as a way to classify the complex fluids, *J. Non-Newtonian Fluid Mech.* 107 (2002) 51–65, [https://doi.org/10.1016/S0377-0257\(02\)00141-6](https://doi.org/10.1016/S0377-0257(02)00141-6).
- A.J. Giacomini, J.M. Dealy, Large-amplitude oscillatory shear, *Techniques in rheological measurement*, Springer 1993, pp. 99–121.
- M. Wilhelm, Fourier-transform rheology, *Macromol. Mater. Eng.* 287 (2002) 83–105, <https://doi.org/10.1002/1439-2054>.
- G.B. Folland, *Pure and Applied Undergraduate Texts*, 4, 2009. Providence, RI, USA, ISBN-10: 0-8218-4790-2.
- L.M. Sagis, M. Ramaekers, E. van der Linden, Constitutive equations for an elastic material with anisotropic rigid particles, *Phys. Rev. E* 63 (2001), <https://doi.org/10.1103/PhysRevE.63.051504>, 051504.
- V. Hirschberg, F. Lacroix, M. Wilhelm, D. Rodrigue, Fatigue analysis of brittle polymers via Fourier transform of the stress, *Mech. Mater.* 103100 (2019), <https://doi.org/10.1016/j.mechmat.2019.103100>.
- T. Dötsch, M. Pollard, M. Wilhelm, Kinetics of isothermal crystallization in isotactic polypropylene monitored with rheology and Fourier-transform rheology, *J. Phys. Condens.* 15 (2003) S923, <https://doi.org/10.1088/0953-8984/15/11/316>.
- V. Hirschberg, M. Wilhelm, D. Rodrigue, Fatigue behavior of polystyrene (PS) analyzed from the Fourier transform (FT) of stress response: first evidence of I2/1 (N) and I3/1 (N) as new fingerprints, *Polym. Test.* 60 (2017) 343–350, <https://doi.org/10.1016/j.polymertesting.2017.04.001>.
- S.N. Ganeriwala, C.A. Rotz, Fourier transform mechanical analysis for determining the nonlinear viscoelastic properties of polymers, *Polym. Eng. Sci.* 27 (1987) 165–178, <https://doi.org/10.1002/pen.760270211>.
- R.H. Ewoldt, P. Winter, J. Maxey, G.H. McKinley, Large amplitude oscillatory shear of pseudoplastic and elastoviscoplastic materials, *Rheo. acta* 49 (2010) 191–212, <https://doi.org/10.1007/s00397-009-0403-7>.
- V. Hirschberg, L. Schwab, M. Czip, M. Wilhelm, D. Rodrigue, Influence of molecular properties on the mechanical fatigue of polystyrene (PS) analyzed via Wöhler curves and Fourier Transform rheology, *Polymer* 138 (2018) 1–7, <https://doi.org/10.1016/j.polymer.2018.01.042>.
- L. Jegou, Y. Marco, V. Le Saux, S. Calloch, Fast prediction of the Wöhler curve from heat build-up measurements on Short Fiber Reinforced Plastic, *Int. J. Fatigue* 47 (2013) 259–267, <https://doi.org/10.1016/j.ijfatigue.2012.09.007>.
- H. Sawadogo, S. Panier, S. Hariri, Calorimetric analysis of dissipative effects associated with the fatigue of GFRP composites, *Fatigue Behaviour of Fiber Reinforced Polymers: Experiments and Simulations* 265 (2012).
- X. Tong, X. Chen, J. Xu, C. Sun, W. Liang, Excitation of thermal dissipation of solid propellants during the fatigue process, *Mater. Des.* 128 (2017) 47–55, <https://doi.org/10.1016/j.matdes.2017.04.088>.
- L. Leveuf, Y. Marco, V. Le Saux, L. Navrátil, S. Leclercq, J. Olhagaray, Fast screening of the fatigue properties of thermoplastics reinforced with short carbon fibers based on thermal measurements, *Polym. Test.* 68 (2018) 19–26, <https://doi.org/10.1016/j.polymertesting.2018.03.045>.
- A. Launay, M. Maitournam, Y. Marco, I. Raoult, F. Szymtyka, Cyclic behaviour of short glass fibre reinforced polyamide: experimental study and constitutive equations, *Int. J. Plast.* 27 (2011) 1267–1293, <https://doi.org/10.1016/j.ijplas.2011.02.005>.
- Z. Qi, N. Hu, G. Li, D. Zeng, X. Su, Constitutive modeling for the elastic-viscoplastic behavior of high density polyethylene under cyclic loading, *Int. J. Plast.* 113 (2019) 125–144, <https://doi.org/10.1016/j.ijplas.2018.09.010>.
- A. Pawlak, A. Galeski, Plastic deformation of crystalline polymers: the role of cavitation and crystal plasticity, *Macromolecules* 38 (2005) 9688–9697, <https://doi.org/10.1021/ma050842a>.
- J. Karger-Kocsis, O. Benevolenski, E. Moskala, Toward understanding the stress oscillation phenomenon in polymers due to tensile impact loading, *J. Mater. Sci.* 36 (2001) 3365–3371, <https://doi.org/10.1023/A:1017935323058>.
- W. Mars, A. Fatemi, Factors that affect the fatigue life of rubber: a literature survey, *Rubber Chem. Technol.* 77 (2004) 391–412, <https://doi.org/10.5254/1.3547831>.
- F. Libonati, L. Vergani, Damage assessment of composite materials by means of thermographic analyses, *Compos. B Eng.* 50 (2013) 82–90, <https://doi.org/10.1016/j.compositesb.2013.01.012>.
- G. Pitarresi, E. Patterson, A review of the general theory of thermoelastic stress analysis, *J. Strain Anal. Eng.* 38 (2003) 405–417, <https://doi.org/10.1243/03093240360713469>.
- W.N. Sharpe, *Springer Handbook of Experimental Solid Mechanics*, Springer Science & Business Media, 2008.
- L. Vergani, C. Colombo, F. Libonati, A review of thermographic techniques for damage investigation in composites, *Fract. Struct. Integr. Ann* 8 (2014), <https://doi.org/10.3221/IGF-ESIS.27.01>.
- J.B. Le Cam, A review of the challenges and limitations of full-field measurements applied to large heterogeneous deformations of rubbers, *Strain* 48 (2012) 174–188, <https://doi.org/10.1111/j.1475-1305.2011.00830.x>.
- A. Benaarbia, A. Chrysochoos, G. Robert, Influence of relative humidity and loading frequency on the PA6. 6 cyclic thermomechanical behavior: Part I. mechanical and thermal aspects, *Polym. Test.* 40 (2014) 290–298, <https://doi.org/10.1016/j.polymertesting.2014.09.019>.
- D. van Dusschoten, M. Wilhelm, Increased torque transducer sensitivity via oversampling, *Rheo. acta* 40 (2001) 395–399, <https://doi.org/10.1007/s003970000158>.
- A. Krairi, I. Doghri, J. Schalnath, G. Robert, W. Van Paepegem, Thermo-mechanical coupling of a viscoelastic-viscoplastic model for thermoplastic polymers: thermodynamical derivation and experimental assessment, *Int. J. Plast.* 115 (2019) 154–177, <https://doi.org/10.1016/j.ijplas.2018.11.016>.
- J. Karger-Kocsis, O.I. Benevolenski, E.J. Moskala, Toward understanding the stress oscillation phenomenon in polymers due to tensile impact loading, *J. Mater. Sci.* 36 (2001) 3365–3371, <https://doi.org/10.1023/A:1017935323058>.
- A. Benaarbia, A. Chrysochoos, G. Robert, Fiber orientation effects on heat source distribution in reinforced polyamide 6.6 subjected to low cycle fatigue, *J. Eng. Math.* 90 (2015) 13–36, <https://doi.org/10.1007/s10665-014-9720-7>.
- C. Yu, G. Kang, K. Chen, A hygro-thermo-mechanical coupled cyclic constitutive model for polymers with considering glass transition, *Int. J. Plast.* 89 (2017) 29–65, <https://doi.org/10.1016/j.ijplas.2016.11.001>.
- F. Shen, G. Kang, Y.C. Lam, Y. Liu, K. Zhou, Thermo-elastic-viscoplastic-damage model for self-heating and mechanical behavior of thermoplastic polymers, *Int. J. Plast.* 121 (2019) 227–243, <https://doi.org/10.1016/j.ijplas.2019.06.003>.
- G. La Rosa, A. Risitano, Thermographic methodology for rapid determination of the fatigue limit of materials and mechanical components, *Int. J. Fatig.* 22 (2000) 65–73, [https://doi.org/10.1016/S0142-1123\(99\)00088-2](https://doi.org/10.1016/S0142-1123(99)00088-2).
- Z. Teng, H. Wu, C. Boller, P. Starke, A unified fatigue life calculation based on intrinsic thermal dissipation and microplasticity evolution, *Int. J. Fatig.* 131 (2020), <https://doi.org/10.1016/j.ijfatigue.2019.105370>, 105370.
- V. Le Saux, Y. Marco, S. Calloch, C. Doudard, P. Charrier, Fast evaluation of the fatigue lifetime of rubber-like materials based on a heat build-up protocol and micro-tomography measurements, *Int. J. Fatig.* 32 (2010) 1582–1590, <https://doi.org/10.1016/j.ijfatigue.2010.02.014>.
- C. Cruanes, M.-P. Deffarges, F. Lacroix, S. Méo, Modeling of the thermomechanical behavior of rubbers during fatigue tests from infrared measurements, *Int. J. Fatig.* 126 (2019) 231–240, <https://doi.org/10.1016/j.ijfatigue.2019.04.035>.
- I. El Sawi, Z. Fawaz, R. Zitounne, H. Bougherara, An investigation of the damage mechanisms and fatigue life diagrams of flax fiber-reinforced polymer laminates, *J. Mater. Sci.* 49 (2014) 2338–2346, <https://doi.org/10.1007/s10853-013-7934-0>.
- W. Luo, Y. Huang, B. Yin, X. Jiang, X. Hu, Fatigue life assessment of filled rubber by hysteresis induced self-heating temperature, *Polymers* 12 (2020) 846, <https://doi.org/10.3390/polym12040846>.
- S.A. Grammatikos, E.Z. Kordatos, T.E. Matikas, A.S. Paipetis, On the fatigue response of a bonded repaired aerospace composite using thermography, *Compos. Struct.* 188 (2018) 461–469, <https://doi.org/10.1016/j.compstruct.2018.01.035>.
- R. Plum, J. Medgenberg, M. Merzbacher, T. Ummerhofer, *Extended Thermoelastic Stress Analysis Applied to Carbon Steel and CFRP*, 2nd International Symposium on NDT in Aerospace, 2010.